

## Propagation Effects in Carbon Nanoelectronics

Ehsan. Hosseini\*

*Sama Technical And Vocational Training College, Islamic Azad University, Tehran Branch,  
Tehran, Iran*

Received 14 Jan. 2014; Revised 3 Oct. 2014; Accepted 21 Jan. 2015

### Abstract

This research examines the ingredients of Cobalt-60 propagation on the electrical attributes of single-walled carbon nanotube and (G-FETs). The research observes significant variances in the radiation response of instruments depending on their propagation environment, and corroborate under controlled conditions, standard dielectric hardening approaches are useable to carbon nanoelectronics devices.

**Keywords:** Radiation; Mobility; Field effect transistors (FETs).

**PACS:** 61.82.Fk; 72.20.Ee; 85.75.Hh.

### 1. Introduction

The unexampled attributes of carbon nanomaterials, in specific single-walled carbon nanotubes (SWCNTs) and graphene, have garnered much attention due to their potential composition into high-performance devices. Recent laboratory-demonstrated threshold frequencies of 80 GHz (SWCNT based) and 100 GHz (graphene based) field-effect transistors (FETs) establish their position among extremely high-mobility materials. Their high mobility and unique ambipolar transport behavior may also prove useful in other analog devices such as power amplifiers, high-frequency mixers, and radio receivers. It is clear that carbon nanoelectronics will enable, in the near future, leap-ahead technologies to address the needs of terrestrial and space-bound systems. It is imperative that the radiation response and methods for radiation hardening be considered in parallel with device development to ensure reliability in harsh environments.

Many theoretical and experimental studies of SWCNTs, and to a lesser extent graphene, have investigated the effects of ionizing radiation on the crystalline structure of these materials [1–3]. The results indicate that ionizing radiation can damage the crystalline lattice by creating defects, although the defect formation probability strongly depends on the energy, mass, and angle of the incident ionizing radiation. Recent studies which monitor the electronic transport properties of carbon-based FETs support these conclusions, that is, a high tolerance to proton irradiation (e.g., SWCNT-FETs, graphene-FETs [4]) or high-energy photon irradiation (e.g., SWCNT [5–11], graphene-FETs [9–10]), where the transport properties of the carbon nanostructures are maintained. However, the overall device response to irradiation is mixed. Some studies show enhanced drain currents (e.g.,

---

\* ) For Correspondence, Tel: + (98) 9122440475, E-mail: Hosseiny.e@gmail.com.

These assorted results motivate the need for utilizing standardized test structures and controlling the experimental conditions to allow for a systematic evaluation of the radiation response of the materials and devices independent of extrinsic effects.

The current study illustrates the sensitivities of carbon nanoelectronic devices to total ionizing dose (TID) effects caused by both intrinsic and extrinsic factors. I begin by comparing the effects of TID on a back-gated graphene FET irradiated in vacuum and in air. I then highlight an approach to increasing the performance and radiation tolerance of SWCNT thin-film-transistors (TFTs) using thinned, high- $\kappa$  gate dielectrics.

## 2. Experimental Section

The preparation of SWCNT thin films (98% semiconducting-enriched, NanoIntegris, Inc.) and subsequent SWCNT-TFT photolithographic processing closely follow our previously reported procedure found in ref. [5,8]. For our back-gated graphene FETs, I grow and transfer graphene films following methods described by Li *et al.*, [11] and use similar photolithographic processing as in Reference [5]. Briefly, graphene is grown using chemical vapor deposition (CVD) on Cu foils at 1000 °C in a horizontal tube furnace in flowing H<sub>2</sub> and CH<sub>4</sub>. Following growth, graphene is transferred using the following steps: (i) spin-on a protective poly(methyl methacrylate) (PMMA) film; (ii) etch the Cu foil; (iii) transfer the floating PMMA-coated graphene to a substrate of choice; and (iv) remove the PMMA by submersion in an acetone bath. The use of transferred films in the preparation of devices allows us to change the substrate material and structure independently from the carbon nanomaterials. I perform Raman spectroscopy (laser wavelength of 532 nm) of the graphene channel material pre- and post Co-60 irradiation to assess changes in defect concentration in graphene.

### 2.1 Back-Gated Device Structures

The standard back-gated structure depicted in Figure 1a is commonly used to study the electrical transport properties of SWCNTs and graphene. The structure allows for rapid fabrication of devices with variable dimensions. Furthermore, any semiconductor or metal substrate with an insulating dielectric layer may serve as the global back-gate electrode to modulate the Fermi level of the carbon active layer. The devices studied here use thermally grown SiO<sub>2</sub> on p<sup>+</sup>-Si as the starting substrate.

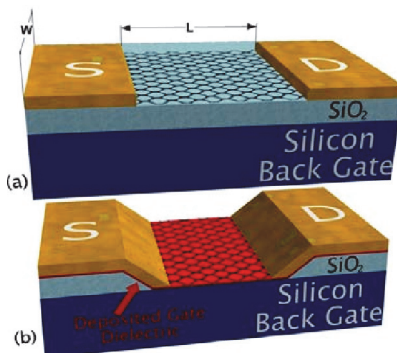


Fig. 1: (a) : Schematic depicting a standard back-gated graphene (FET) and (b) a locally etched back-gated FET structure with a deposited dielectric layer. For the single-walled carbon nanotube (SWCNT)-thin-film-transistors (TFTs), a thin mesh of SWCNTs replaces the graphene film depicted here.

Though versatile, these back-gated structures are not optimized for high performance since they typically have thick dielectric layers ( $>1000\text{ \AA}$ ) resulting in low gate capacitance, and thus, require biases of tens-of-volts to fully saturate or pinch-off the drain current. Furthermore, thick dielectric layers are highly susceptible to radiation induced charge build-up, which is known to cause threshold voltage shifts and increased leakage in metal oxide semiconductor (MOS) devices [12]. To mitigate these effects, the dielectric layer was locally etched in the active region of the back-gated FET, which is depicted in Figure 1b. Later a gate dielectric material (e.g.,  $\text{Al}_2\text{O}_3$  or  $\text{Si}_3\text{N}_4$ ; depicted in red in Figure 1b) was deposited over the entire substrate with a thickness controlled by growth. This design feature is important since high quality dielectric layers deposited directly onto SWCNTs or graphene for use as a top gate electrode are still under development. Using the locally etched back-gated (LEBG) structure allows us to maintain the properties of the transferred carbon nanomaterial channel.

## 2.2 $\text{SiO}_2$ Local Etching

The channel regions of the LEBG devices were patterned using standard photolithographic procedures. These substrates are etched for 1–3 min in buffered oxide etch (BOE) (7:1  $\text{NH}_4\text{F}:\text{HF}$ ), followed by a short~1 min rinse in flowing deionized water. This etchant produces smooth hydrogen-terminated Si terraces [13,14], thereby providing a controlled surface for subsequent dielectric layer deposition.

## 2.3 $\text{Si}_3\text{N}_4$ Plasma Enhanced Chemical Vapor Deposition (PECVD)

$\text{Si}_3\text{N}_4$  films on LEBG substrates were deposited and BOE etched control wafers for optical and electrical characterization using an Oxford Instruments Plasma Pro™ System 100. Freshly prepared substrates are loaded, pumped to  $5 \times 10^{-6}$  Torr and preheated to 350 °C for 10 min.  $\text{Si}_3\text{N}_4$  deposition proceeds at a pressure of 2 Torr with an  $\text{N}_2$  carrier gas, and  $\text{SiH}_4$  and  $\text{NH}_4$  as the Si and N precursors, respectively. An index of refraction of 1.97 at 633 nm was obtained based on fitted reflectance measurements indicating nearly stoichiometric  $\text{Si}_3\text{N}_4$ . Following SWCNT thin-film deposition, annealing the structures in air at 300 °C for 16 h introduces oxygen into the nitride layer transforming it into silicon oxynitride (SiON) with an index of refraction of 1.75 at 633. On control samples, Ti/Au contact pads were deposited to perform capacitance and electrical breakdown measurements. For a 23 nm SiON film, an average dielectric constant of  $\epsilon_r = 5.5$  at 1 MHz and dc-breakdown fields in excess of 8 MV/cm [8] were obtained.

## 2.4 $\text{Al}_2\text{O}_3$ Atomic Layer Deposition (ALD)

$\text{Al}_2\text{O}_3$  films on LEBG substrates and BOE etched control wafers for optical and electrical characterization were deposited using an Oxford Instruments FlexAL system. In a similar fashion as the  $\text{Si}_3\text{N}_4$ , I deposit  $\text{Al}_2\text{O}_3$  on freshly prepared substrates, which are loaded, pumped, and preheated to 300 °C. The growth proceeds at this temperature as trimethyl aluminum (TMA) the Al precursor and oxygen plasma are alternatingly pulsed into the growth chamber. Ti/Au contact pads were deposited to perform capacitance and electrical breakdown measurements. For a 32 nm  $\text{Al}_2\text{O}_3$  film, I obtained an average dielectric constant of  $\epsilon_r = 8.3$  at 1 MHz and dc-breakdown fields in excess of 10 MV/cm.

### 3. Results and Discussion

#### 3.1 Characterizing Air Sensitivity of Carbon Electronics

Recently, observed that the response of SWCNT-TFTs to Co-60 exposure is highly dependent on the local environment of the device during irradiation [5]. It is reported here a similar experiment on a standard back-gated graphene FET with a 250 nm SiO<sub>2</sub> gate oxide, channel length of 15 μm, channel width of 60 μm, and a positive gate bias of 5 V during irradiation. Figure 2a illustrates the TID dependent transfer characteristics of the wire bonded standard back-gated graphene FET measured in static vacuum. The pre-irradiation transfer characteristics (black trace labeled 0 krad(Si)) were measured immediately before the first TID exposure (1 krad = 10 Gy). Control measurements were performed which yielded constant transfer characteristics for the device held in the sample chamber under static vacuum prior to irradiation. A large shift in the transfer characteristics (towards negative  $V_g$ ) was observed following a TID of 20 krad(Si), which proceeds with further dosing. Following a TID of 40 krad(Si), the Dirac point becomes apparent at  $V_g = 73$  V along with the onset of the electron transport for  $V_g > 73$  V. These results are consistent with the hole trapping in the SiO<sub>2</sub>, which increases the Fermi level closer to mid-gap. Following the initial Co-60 irradiation up to 5 Mrad(Si), The device was exposed to air for 15 m then repeated the experiment with the same device in an air ambient as shown in Figure 2b. During the 15 m repose, the transfer characteristics shift towards positive gate voltage, resulting from room temperature annealing of the radiation-induced trapped charges and due to adsorption of molecular species from the air. Additional irradiation in an air ambient causes the transfer characteristics to shift further towards positive gate bias, the opposite of what is observed when irradiated under vacuum. This indicates that molecular species from the air, namely oxygen and water, overpower the effects of SiO<sub>2</sub> trapped holes and decrease the Fermi level promoting the hole doping in the channel [10].

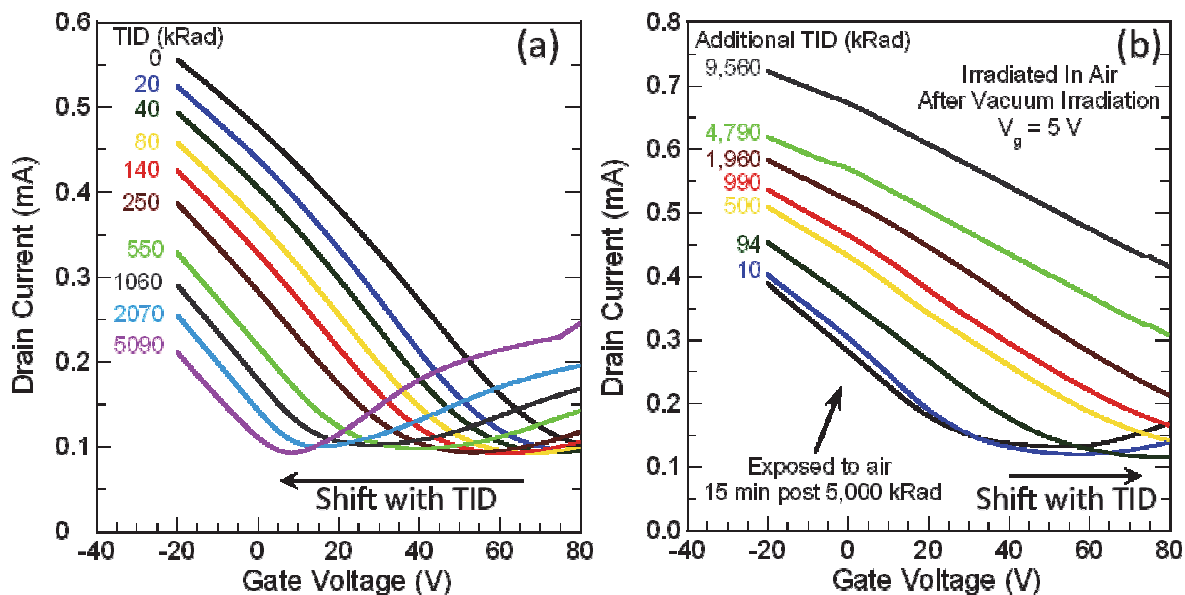


Fig. 2 (a) : Transfer characteristics of a back-gated graphene-FET with incremental total ionizing dose; (b) Transfer characteristics of the same device following 15 min of air exposure (black curve) and with additional total ionizing dose (TID).

Using the standard long-channel field effect mobility equation:  $\mu_{FE} = \frac{L/W}{C_{ox}V_{DS}} \frac{dI_D}{dV_G}$ , where L is the channel length, W is the width  $C_{ox}$  is the oxide capacitance,  $I_D$  is the drain current, and  $V_G$  is the gate voltage. The peak  $\mu_{FE}$  from the transfer curves were calculated as plotted versus TID in Figure 3a for the graphene FET irradiated in vacuum and air. When irradiated in vacuum, the hole initially degrades from  $1090 \text{ cm}^2/\text{Vs}$  to  $980 \text{ cm}^2/\text{Vs}$  following a TID of 200 krad(Si), recovers slightly then degrades again reaching a minimum mobility of  $896 \text{ cm}^2/\text{Vs}$  after a TID of 5 Mrad(Si). During the 15 m repose, the mobility recovers considerably from the low of  $896 \text{ cm}^2/\text{Vs}$  increasing to  $1126 \text{ cm}^2/\text{Vs}$  exceeding the pre-irradiation mobility. With increasing TID exposure in air, the mobility decreases to  $907 \text{ cm}^2/\text{Vs}$  after a TID of 100 krad(Si), then after a brief plateau, degrades to  $663 \text{ cm}^2/\text{Vs}$  following a total (additional) TID of 5 Mrad(Si) in air. The variation in  $\sigma_{min}$  with TID was also plotted for the transfer curves measured in vacuum in Figure 3a (lower right y-axis). In this figure,  $\sigma_{min}$  displays non-monotonic behavior that approximately follows that of the mobility (measured in vacuum). The  $\sigma_{min}$  provides a relative measure of the charge inhomogeneity at the graphene-substrate interface resulting from trapped charges in  $\text{SiO}_2$  and adsorbed impurities including oxygen, moisture and photoresist residues[15].

The initial decrease in  $\sigma_{min}$  with TID reflects the increasing trapped charge density and magnitude of charge potential fluctuations (*i.e.*, electron-hole puddles) within the graphene channel. These fluctuations restrict current flow in the graphene channel, which favors transport through regions of unperturbed potential, and is expected to reduce the mobility as observed. Following a TID of 200-500 krad(Si), the  $\sigma_{min}$  and  $\mu_{FE}$  begin to recover. This behavior was attributed to a reorganization of the potential fluctuations in the graphene, potentially resulting in a correlated charge distribution in the  $\text{SiO}_2$  [16] or rearrangement of mobile surface adsorbates, though additional work is needed to confirm this mechanism.

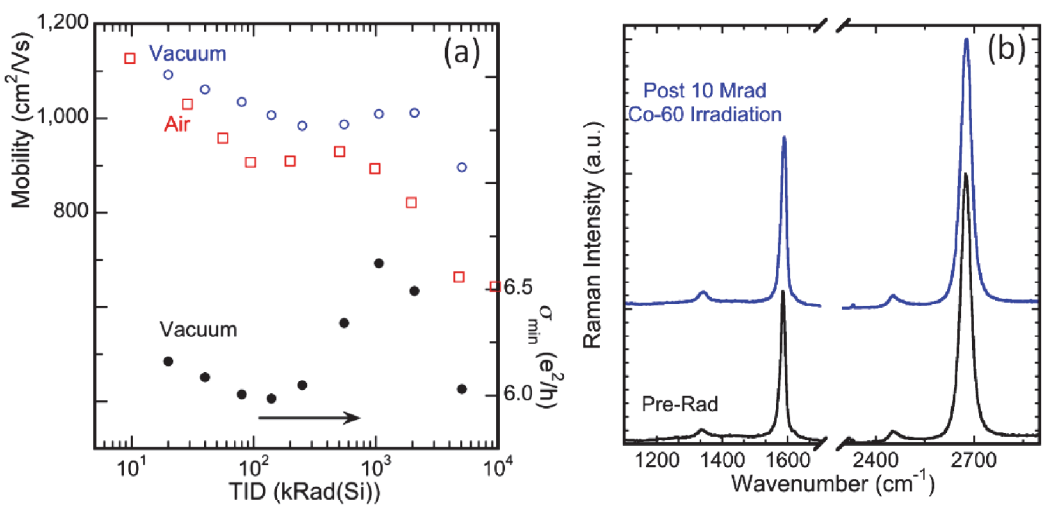


Fig. 3 (a) : Field effect mobility as a function of TID for a graphene-FET irradiated in vacuum (blue, open circles) and in air (red, open squares), along with the minimum conductivity (*i.e.*, the conductivity at the Dirac point) for the transfer characteristics measured in vacuum; (b) Representative Raman spectra of the graphene FET both pre- and post 10 Mrad(Si) irradiation.

In Figure 3b, provided characteristic pre- and post 10 Mrad(Si) Co-60 irradiation Raman spectra of the graphene device measured in Figure 2. I measure a 2D-band ( $2670\text{ cm}^{-1}$ ) to G-band ( $1580\text{ cm}^{-1}$ ) peak intensity ratio of 1.5, which is characteristic of single layer graphene on SiO<sub>2</sub> [17]. The D-band mode ( $\sim 1345\text{ cm}^{-1}$ ) results from disorder in the graphene, potentially arising from defects, edges, wrinkles, or residual PMMA resist, but the relatively low intensity indicates the disorder is minimal. Furthermore, observed no significant difference in the D-band intensity following following irradiation indicating that the changes observed in the graphene FETs due to Co-60 irradiation result from trapped charges in the SiO<sub>2</sub> gate oxide and not due to changes in lattice defect concentration

### 3.2 SiON and Al<sub>2</sub>O<sub>3</sub> Gate Dielectrics with the Locally Etched Back-Gated Structure (SWCNT-TFTs)

In Figure 4a, the transfer characteristics of two LEBG SWCNT-TFTs were compared with either a 32 nm SiON or a 32 nm Al<sub>2</sub>O<sub>3</sub> gate dielectric layer, 2  $\mu\text{m}$  channel lengths, and 32  $\mu\text{m}$  channel widths. Both devices are representative of the devices with drain current  $I_{d,\text{on}}/I_{d,\text{off}}$  greater than  $10^4$  (about 20 devices for each gate dielectric). For both dielectric layers, A maximum drain current of  $1 \times 10^{-7}\text{ A}$  was perceived and a consistently lower minimum drain current for the SiON (about  $10\times$  lower). The larger off-current may result from the onset of electron transport in the Al<sub>2</sub>O<sub>3</sub> device reflecting the ambipolar transport properties of SWCNTs [18]. A different level of adsorbed water due to the different surface energies of Al<sub>2</sub>O<sub>3</sub> and Si<sub>3</sub>N<sub>4</sub> may cause this, which is supported by the fact that similar ambipolar behavior is observed in LEBG SWCNT-TFTs with a SiON gate dielectric following vacuum annealing at 125 °C and  $1 \times 10^{-5}$  Torr (see Figure 4b).

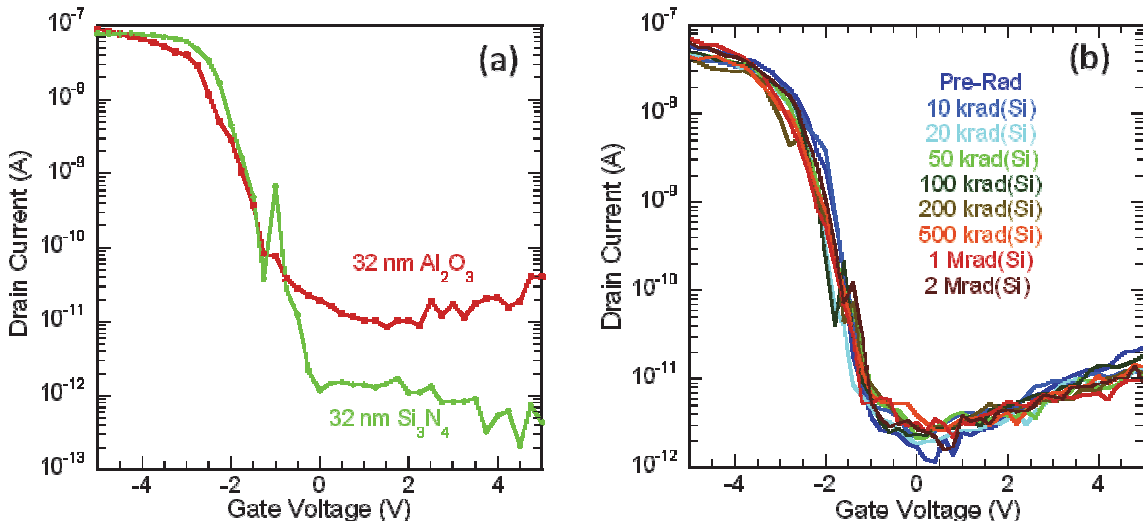


Fig 4. (a) : Transfer characteristics of SWCNT-TFTs with 32 nm Al<sub>2</sub>O<sub>3</sub> (red) and with 32 nm SiON (green) gate dielectric layers; (b) The radiation response of SWCNT-TFT with a 23 nm SiON gate dielectric layer.

In Figure 4b, investigated the effects of Co-60 irradiation for a LEBG SWCNT-FET with a 23 nm SiON gate oxide and channel length and width of 2  $\mu\text{m}$  and 16  $\mu\text{m}$ , respectively, biased with a 0.25 MV/cm gate field during irradiation. By scaling the gate dielectric material to 23 nm observed that essentially no effect of Co-60 irradiation on the

transfer characteristics up to a TID of 2 Mrad(Si). A maximum shift in the threshold voltage of  $-0.25$  V was observed at a TID of 100 krad(Si) after which the transfer characteristics begin to shift back towards positive  $V_g$  values. The stability in  $V_g$  results from lower trapped charge accumulation in the thin SiON layer—the thinner layer allows more carriers to escape by tunneling or through field assisted transport [19-21]. Furthermore, the trapping characteristics of SiON are distinct from SiO<sub>2</sub> and favor electron trapping over hole trapping [12]. Therefore, the positive shift in threshold voltage was attributed to electron traps in the SiON [8], although it is not possible to completely rule out some molecular doping during irradiation in static vacuum conditions.

The data presented here is promising evidence towards hardening carbon nanoelectronics against TID exposure. Therefore, our future investigations are aimed at maintaining the radiation tolerance levels while simultaneously improving device performance and reducing the susceptibility to atmospheric doping effects.

#### 4. Conclusions

The sensitivities of graphene FETs, including shifting Dirac point and mobility degradation have illustrated, due to TID exposure as well as the compounded effects caused by doping from molecular adsorbates. A correlation observed between the minimum conductivity, and hole mobility, , both of which vary non-monotonically with increasing TID. This behavior was attributed to an evolving electron-hole puddle distribution, controlled by SiO<sub>2</sub> trapped charges and mobile surface impurities. Using a locally etched back-gate region, a device structure that can leverage standard hardening approaches have created including the use of alternative dielectric materials and thinner gate dielectric layers. This has led to the demonstration of a SWCNT-TFT which is nearly unaffected by ionizing radiation up to a total dose of 2 Mrad(Si).

#### References

- [1] C.D.Cress, C.M.Schauerman, B.J.Landi, S.R.Messenger, R.P.Raffaelle, R.J.Walters, *Radiation effects in single-walled carbon nanotube*, papers. J. Appl. Phys., **107**, 014316 (2010)
- [2] H. S. Kim, T. Banks, J.A. Rogers, A.A. Pesetski, J.E.Baumgardner, S.V.Krishnaswamy, H. Zhang, Radio frequency analog electronics based on carbon nanotube transistors, Proc. Natl. Acad. Sci., **105**, 1405–1409. USA (2008)
- [3] C. Kocabas, H. S. Kim, T. Banks, J.A. Rogers, A.A. Pesetski, J.E. Baumgardner, S.V. Krishnaswamy, H. Zhang, Radio frequency analog electronics based on carbon nanotube transistors, Proc. Natl. Acad. Sci., **105**, 1405–1409. USA (2008)
- [4] G.Ko, H.Y.Kim, F.Ren, S.J.Pearton, Electrical characterization of 5 MeV proton-irradiated few layer graphene, Electrochem. Solid State Lett, **13**, K32–K34.( 2010)
- [5] C.D.Cress, J.J.McMorrow, J.T.Robinson, Radiation effects in single-walled carbon nanotube thin-film-transistors, IEEE Trans. Nucl. Sci., **57**, 3040–3045. (2010)
- [6] D. Zhang, K .Wang, J. Tong, B. Xia, Multi-walled Carbon Nanotube Film Sensor for Ethanol Gas Detection. Telkomnika.; **11** (10): pp.6120-6126, (2013)
- [7] S.A.Vitusevich, V.A. Sydoruk, M.V. Petrychuk, B.A. Danilchenko, N. Klein, A. Offenhäusser, A. Ural, G. Bosman, Transport properties of single-walled carbon nanotube transistors after gamma radiation treatment, J. Appl. Phys., **107**, 063701. (2010)

- [8] C.D. Cress, J.J. McMorrow, J.T. Robinson, A.L.Friedman, H.L.Hughes, B.D.Weaver, B.J. Landi, Total ionizing dose-hardened carbon nanotube thin-film transistors with silicon oxynitride gate dielectrics, MRS Commun., **1**, 27–31.( 2011)
- [9] R.D. Schrimpf, D.M. Fleetwood, M.L. Alles, R.A. Reed, G.Lucovsky, Radiation effects in new materials for nano-devices. Microelectron. Eng., **88**, 1–6. (2011)
- [10] E.X. Zhang, A.K.M. Newaz, B.Wang, S. Bhandaru, C.X. Zhang, D.M. Fleetwood, K.I. Bolotin, Low-energy X-ray and ozone-exposure induced defect formation in graphene materials and devices, IEEE Trans. Nucl. Sci., **58**, 2961–2967. (2011)
- [11] X. Li, Y. Zhu, W. Cai, M. Borysiak, B. Han, D. Chen, R. Piner,; Colomba, Transfer of large-area graphene films for high-performance transparent conductive electrodes, Nano Lett., **9**, 4359–4363. (2009)
- [12] T. Oldham, Ionizing Radiation Effects in MOS Oxides; World Scientific: Singapore, (1999)
- [13] V.Le Thanh, D. Bouchier, D. Débarre, Fabrication of SiGe quantum dots on a Si(100) surface, Phys. Rev. B, **56**, 10505–10510. (1997)
- [14] G.J. Pietsch, Hydrogen on Si Ubiquitous surface termination after wet-chemical processing. Appl. Phys. A, **60**, 347–363. (1995)
- [15] Y. Sui, T. Low, M. Lundstrom, J. Appenzeller, Signatures of disorder in the minimum conductivity of graphene, Nano Lett., **11**, 1319–1322. (2011)
- [16] Yan, J.; Fuhrer, M. Correlated charged impurity scattering in graphene. Phys. Rev. Lett., **107**, 206601 ( 2011)
- [17] X. Li, Cai, W. An, J. Kim, S. Nah, J. Yang, D. R. Piner; A. Velamakanni, I. Jung, Large-area synthesis of high-quality and uniform graphene films on copper foils, Science, **324**, 1312–1314. (2009)
- [18] A. Javey, M.Shim, H.Dai, Electrical properties and devices of large-diameter single-walled carbon nanotubes. Appl. Phys. Lett, **80**, 1064. (2002)
- [19] N. Saks; M. Ancona, J. Modolo, Radiation Effects in MOS Capacitors with Very Thin Oxides at 80 °K. IEEE Trans. Nucl. Sci., **31**, 1249–1255. (1984)
- [20] *S. H. Alias, N.A. Buang, A. M. Yusof and M. L. Ibrahim*, Aspirin adsorption on multiwalled carbon nanotubes and its release characteristics in simulated body fluid, The international journal of nanoelectronics and materials (IJNeAM), **7** (1), 35-43, (2014)
- [21] *A. Dan, T. K. Kundu, D. Chakravorty*, Surface conductivity of aligned carbon nanotubes in silica gel, The International Journal of Nanoelectronics and Materials (IJNeAM), **6** (1), 67-72, (2013)